



## Robust *Aspergillus terreus* biofilm supported on graphene oxide/hematite-nanocomposites for adsorption of anthraquinone dye

Asmaa M.M. Mawad, Naeima M.H. Yousef, Ahmed A.M. Shoreit\*

Faculty of Science, Botany and Microbiology Department, Assiut University, Assiut 71516, Egypt, Tel. +20 1069830324; emails: [a.mawad@aun.edu.eg](mailto:a.mawad@aun.edu.eg), [asmaa\\_botany@yahoo.com](mailto:asmaa_botany@yahoo.com) (A.M.M. Mawad), [naeima@sci.au.edu.eg](mailto:naeima@sci.au.edu.eg) (N.M.H. Yousef), Tel. +20 1003406161; email: [ashoreit1968@yahoo.com](mailto:ashoreit1968@yahoo.com) (A.A.M. Shoreit)

Received 21 April 2015; Accepted 30 December 2015

### ABSTRACT

Hematite/graphene oxide (FGO) nanocomposites were used as a supporting surface for the fungus *Aspergillus terreus* AUMC-050 to form AFGO biofilm. Different techniques were used for characterization of nanocomposites and biofilm such as IR, Fourier transform infrared, Scanning electron microscopy, Transmittance Electron Microscopic, Brunauer–Emmett–Teller surface area, and Raman Spectroscopy. The effect of initial dye concentration (0–300 mg/L), contact time (0–80 min), pH values (2.0–8.0), and temperature (10–50°C) was studied. The maximum adsorption capacity of dye using AFGO biofilm was 160 mg dye/g at pH 2.0, and the contact time was 50 min. The best fitted equilibrium and kinetic model were found to be Langmuir and pseudo-first order, respectively. Various thermodynamic parameters were evaluated to determine the nature of biosorption process. The negative value of  $\Delta G$  and  $\Delta H^\circ$  indicated spontaneity and exothermic behavior of the adsorption process. Using of microbial biofilm supported on nanocomposite material is a new approach for adsorption of dyes from water body.

*Keywords:* Acid Blue 25; *Aspergillus terreus*; Biosorption; Graphene oxide; Nanocomposites

### 1. Introduction

Synthetic dyestuff is a group of organic pollutants that are applied mainly in textile, printing, paper industries, and dye houses. Acid Blue 25 is an anthraquinone anionic azo dye that is characterized by a high mutagenicity, carcinogenicity due to complex aromatic structures, resistance to light, and high stability in the environment [1,2]. Adsorption has been proved to be one of the most effective technologies used for wastewater treatments and synthetic dye

removal. It is also considered a simple and economical method compared to other traditional methods [3,4].

In the field of adsorption methods, carbon-based materials rank as the most effective material due to their regenerability and stability. Graphene, a thin layer of a pure carbon, has a worldwide attention since it was discovered in the twenty-first century due to its unique properties. Graphene oxide (GO) nanosheets were prepared from graphite powder after oxidation and sonication [5]. As a carbon-based material, GO characterized by a thin planner and two-dimensional sheets with a high aspect ratio, large number of reactive oxygen species on its surface (such as epoxy, carboxyl, and hydroxyl groups), and strong

\*Corresponding author.

$\pi$ - $\pi$  interaction [4]. These distinguished features make it comparatively stable, hydrophilic, and helps it to react easily in aqueous solution. Thus, it is the most widely used material in the field of wastewater treatment [6]. The major advantages of GO nanosheet are low cost and more effective adsorbent instead of many organic materials such as active carbon. Currently, GO and its derivatives are used in many applications such as adsorption of  $H_2$  storage, sensors for detecting individual gas molecule [7], and removal of reactive dyes and heavy metals [8,9]. However, the main disadvantage of GO is that it is difficult to separate from aqueous solution using filtration or centrifugation after adsorption due to its small particle size and high dispersibility [10].

Magnetic iron oxide nanoparticles attract attention of researchers due to its wide range of potential applications including magnetic fluids, gas sensors, catalysis, biomedicine/biotechnology, magnetic resonance imaging (MRI), and data storage. Thermodynamically, hematite ( $\alpha$ - $Fe_2O_3$ ) is the most stable member in the family of iron(III) oxides. Many literature discussed the usage of  $Fe_3O_4$ -GO for adsorption of different types of dyes [10]. The magnetic ( $Fe_3O_4$ ) baker's yeast biomass was used for biosorption of methyl violet [11]. However, so far no literature have mentioned the use of microbe supported onto GO or its derivatives for biosorption studies.

Microorganisms, including bacteria, yeast, fungi, and algae, were used as biosorbents to diminish the toxicity and remove the dyes from industrial effluents due to their safe performance and low cost [12,13]. Unfortunately, the usage of microbial biomass as a biosorbent of different pollutants is quietly limited due to its small particle size and low mechanical strength.

In order to overcome these problems, the microbial biofilm supported on chemical materials was used to increase adsorption efficiency. The benefits of biofilm technology are controlling particle size, capability of regeneration, high biomass loadings, high mechanical strength, and easy to remove from aqueous solution [14]. For this reason, the combination between the microorganism and hematite/GO nanocomposite may enhance the adsorption capability of microorganism and GO along with the merit of easy separation due to the presence of hematite ( $\alpha$ - $Fe_2O_3$ ), could lead to a high efficient dye adsorption capacity from aqueous solutions.

So, this study was aimed to: (i) isolation and identification fungal strain with high adsorption capability, (ii) synthesis and characterization GO nanosheet,  $\alpha$ - $Fe_2O_3$  (hematite) nanoparticles, and FGO nanocomposite, and (iii) prepare the biofilm of *Aspergillus terreus* (AUMC-050) supported on hematite/GO nanocomposites and determine the anionic dye

adsorption performance of this biofilm with special references to adsorption kinetics, isotherms, and thermodynamics.

## 2. Materials and methods

### 2.1. Sample collection

One sample was collected from Industrial dye effluent located in Spinning and Textile Factory in 10th of Ramadan city, Industrial zone no. 1, Cairo, Egypt.

### 2.2. Enrichment, isolation, and identification of dye decolorizing fungi

Enrichment technique was used for the enumeration and isolation of dye decolorizing fungi. About 10 mL of sample was suspended in 90 ml mineral basal salt medium (MBS) [15] supplemented with 1 g/L of glucose, 50 mg/L AB 25, and pH was adjusted to  $5.0 \pm 0.2$  with KOH. Flasks were incubated on an orbital shaker at 150 rpm at  $28^\circ C$ . After 7 d of incubation, an aliquot of 10% enriched cultures was transferred into another 250-ml conical flasks containing 90 ml fresh autoclaved MBS medium supplemented with previously mentioned dye. This step was repeated three times to attain well-adapted dye decolorizing fungal species. Fungal strains were isolated on MBS agar plates. Colonies with different morphologies were individually selected and evaluated for their dye decolorizing abilities. Pure strain was designated as AUMC-050, identified according to [16] and selected for further studies based on high removal ability of the dye.

### 2.3. Adsorbate preparation

AB 25 dye was purchased from a Local Company. Its chemical formula and molecular weight are  $C_{20}H_{13}N_2NaO_5S$  and 416.38 g/mol, respectively. The C.I number is 62055, and the percentage of dye purity is 93%. The AB 25 was scanned by UV-spectrophotometer to determine the maximum absorbance. The standard calibration curve was performed and measured at  $\lambda_{max}$  600 nm using different concentrations of AB 25 (5–300 mg/L).

### 2.4. Adsorbents preparation

#### 2.4.1. Fungal biomass

The growing fungal biomass of *A. terreus* AUMC-10516 was collected after 7 d at  $28^\circ C$  under static condition. It was washed and oven-dried at  $80^\circ C$  for 24 h.

#### 2.4.2. GO nanosheets

GO was prepared from graphite powder as the method described by [10]. One gram of graphite powder was added to 23 mL of concentrated H<sub>2</sub>SO<sub>4</sub> in an ice bath. To the last mixture, 3 g of KMnO<sub>4</sub> was added slowly with stirring and cooling to maintain the temperature below 20°C. The temperature of the mixture was raised to 35°C for 30 min followed by slow adding of 46 mL of deionized water and then the temperature was increased to 98°C. After 15 min, 140 mL of deionized water was added followed by 10 mL of 30% H<sub>2</sub>O<sub>2</sub> solution. The solid product was separated by centrifugation at 4,000 rpm and washed three times repeatedly with 5% HCl solution and distilled water. The product was then filtered and washed with acetone to make it moisture free. The solid precipitates of GO were filtered through a 0.45- $\mu$ m nylon membrane filter and then dried under vacuum at 60°C. To obtain GO nanosheets, the graphite oxide was suspended in deionized water and exfoliated through ultrasonication for 30 min.

#### 2.4.3. $\alpha$ -Fe<sub>2</sub>O<sub>3</sub> (hematite)

$\alpha$ -Fe<sub>2</sub>O<sub>3</sub> (hematite) nanoparticles were prepared from ferric nitrate, Fe(NO<sub>3</sub>)<sub>2</sub>·9H<sub>2</sub>O, and glycine. In a typical procedure, the required amounts of ferric nitrate and glycine for glycine/ferric nitrate molar ratio of 1 were weighed to the nearest milligram. Ferric nitrate and glycine were dissolved in 100 mL of distilled water to form a pink homogeneous solution; the solution was then transferred to a flask fitted with a water condenser, after that it was heated to 100°C with stirring. The product obtained was evaporated by heating over a hotplate at 100°C. Lastly, the dried precursor was calcined in a muffle furnace at 400°C for 3 h in a static air atmosphere.

#### 2.4.4. $\alpha$ -Fe<sub>2</sub>O<sub>3</sub>/GO nanocomposites (FGO)

Synthesis of  $\alpha$ -Fe<sub>2</sub>O<sub>3</sub>/GO nanocomposites (FGO) was performed by the impregnation method as described by Kyzas et al. [10]. About 0.3 g GO was dispersed in 300 mL distilled water and then sonicated for 30 min in order GO nanosheet to be formed. An amount of 0.3 g of Fe<sub>2</sub>O<sub>3</sub> nanoparticles was added to GO nanosheets and sonicated for 30 min to obtain FGO nanocomposites which were collected by centrifuging and freeze-dried.

#### 2.4.5. Biofilm of *A. terreus* supported on FGO nanocomposite

The biofilm was prepared by shaking method. About 0.3 g of FGO was suspended in 50 mL deionized water followed by ultrasonication for 30 min. About 0.3 g of dry biomass of AUMC-050 added to it. The mixture was shaking at 150 rpm for 48 h at 30°C. Then, the latter was centrifuged and freeze-dried to obtain constant weight [17].

#### 2.5. Characterization of the individual adsorbent

X-ray diffraction (XRD) analysis was carried out using a Model PW 1710 control unit (Philips, New York, NY, USA) with a Cu K $\alpha$ , anode material Cu ( $\lambda = 0.1548$  nm), 40 K.V, 30 M.A, Optics: automatic divergence slit and Beta filtering using a graphite monochromator. The samples were scanned from 4° to 90°. The average crystalline size of the nanoparticles ( $D$ ) was calculated using Debye–Scherrer equation:

$$D = Ks \times \lambda / B \cos \theta \quad (1)$$

where  $Ks$  is a constant ( $K = 0.9$  for Cu K $\alpha$ ),  $\lambda$  (nm) is the wavelength (0.1548 nm for CuK $\alpha$ ),  $B$  is the peak width at half maximum (rad), and  $\theta$  is the diffraction angle. Fourier transform infrared (FTIR) analysis for samples under investigation was performed to give a qualitative and preliminary characterization of the main chemical groups present on AUMC-050, GO and AFGO are responsible for biosorption of AB 25. A 0.01 g of each dried (overnight at 60°C) sample was mixed with 0.1 g KBr and pressed by bench press to get a transparent pellet. This pellet is ready for analyzing by FT-IR Model 470 Shimadzu Corporation adopting KBr disk technique. Scanning electron microscopy (SEM) images were performed at Zeiss Supra 55 VP. The accelerating voltage was 15.00 kV, and the scanning was performed *in situ* on a sample powder. Transmittance electron microscopic (TEM) images were also performed.

Brunauer–Emmett–Teller (BET) surface areas were measured on a Micromeritics ASAP 2020 sorptometer using nitrogen adsorption at 77.4 K. UV–vis absorption spectroscopy was performed on Hitachi U-4100.

Raman spectra were recorded with surface enhanced Raman spectrophotometer (JYHR800)

## 2.6. Adsorption studies

### 2.6.1. Effect of pH

The optimum pH value was performed by analyzing the amount adsorbed (mg/g) of 50 mg/L of dye for each adsorbent over the pH range from 2.0 to 8.0.

### 2.6.2. Effect of contact time and adsorption kinetics

A 20 mg of adsorbent was suspended in 20 ml deionized water consists of AB 25 (50 mg/L). Adsorption was carried out under constant environmental conditions ( $T = 30^{\circ}\text{C}$ ; pH  $2.0 \pm 0.2$  and 150 rpm shaking). Deionized water containing (50 mg/L) dye served as a negative control. Aliquots were withdrawn for each ten-minute intervals during the batch adsorption process to determine the remaining dye concentration. The samples were centrifuged at 10,000 rpm for 15 min, and dye concentration of the supernatant was determined at  $\lambda_{\text{max}}$  600 nm by UV–vis spectrophotometer. The absorbance was converted to concentration using the calibration curve.

The amount of AB 25 adsorbed at equilibrium  $q_e$  (mg/g) was analyzed by the following equation:

$$q_e = (C_o - C_t)V/m \quad (2)$$

where  $C_o$  is the initial concentration of AB 25 (mg/L),  $C_t$  is the concentration of AB 25 at time  $t$  (mg/L),  $V$  is the total volume of the suspension (L), and  $m$  is the mass of adsorbent (g). Pseudo-first-order and pseudo-second-order models were used to calculate  $q_e$  (mg/g).

### 2.6.3. Adsorption isotherm and thermodynamics

Adsorption isotherm was performed at different initial concentration of AB 25 (25, 50, 100, 150, 200, and 300 mg/L) under the fixed environmental conditions that were mentioned before. The Langmuir and Freundlich models were applied to determine the most suitable one for AB 25 biosorption. The change in free energy and thermodynamics of adsorption was determined at different experimental temperatures (5, 10, 20, 30, 40, and  $50^{\circ}\text{C}$ ).

## 2.7. Repetition of batch adsorption experiments

Each experiment was carried out in triplicate to confirm the adsorption rate. For gross error measurements, more repeats of experiments were performed according to the rejection of outliers from statistic treatment of data using SigmaPlot program. The

results presented with error bars were from the average of three repeated measurements from each adsorption experiment.

## 3. Results and discussion

### 3.1. Isolation and identification of dye decolorizing fungi

Among 15 dye decolorizing fungal species, AUMC-050 was selected due to its great capability to decolorize AB 25. The isolate was identified in Assiut University Mycological Center (AUMC) as *A. terreus* based on its color, morphology on solid medium, and certain biochemical activities according to previously described method [16,18].

### 3.2. Characterization of the synthesized adsorbents

The XRD patterns of the GO nanosheet and FGO nanocomposites were demonstrated in (Fig. 1). The diffraction peaks of GO appeared at  $2\theta$  and the particle sizes (nm) were  $10.4^{\circ}$  (3.39) and  $25.2^{\circ}$  (4.94); moreover, the diffraction peaks of FGO were at  $33.3^{\circ}$  (17.29),  $35.56^{\circ}$  (17.86),  $40.8^{\circ}$  (11.18),  $49.5^{\circ}$  (16.96),  $55.3^{\circ}$  (20.14), and  $57.4^{\circ}$  (12.88). The diffraction peak of the crystalline  $\alpha\text{-Fe}_2\text{O}_3$  (hematite) nanoparticle was at  $33.3^{\circ}$ , with an average size approximately 18 nm. The diffraction peaks of GO disappeared, explaining the exfoliation of GO during the preparation of FGO. The appearance of a broad peak at  $24.08^{\circ}$  indicated that  $\alpha\text{-Fe}_2\text{O}_3/\text{GO}$  was formed. So, these results highly agreed with previous results described by Kyzas et al.; [10] however, they prepared  $\text{Fe}_3\text{O}_4/\text{GO}$  nanocomposite (mGOi) as a dye adsorbent. It could be found that the peak of  $\text{Fe}_3\text{O}_4$  was at  $35.56^{\circ}$  with the average size of 18.4 nm, and the GO peak at  $10.3^{\circ}$  was completely disappeared after preparation of mGOi [10].

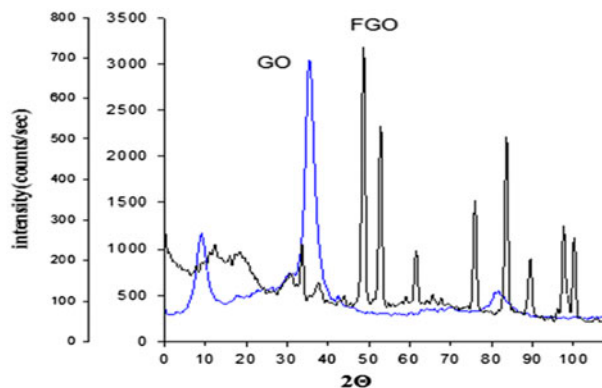


Fig. 1. XRD patterns of FGO (black) and GO (blue).

FTIR spectra of the prepared adsorbent are summarized in Fig. 2. The FTIR spectra of GO showed the presence of a C–O stretch and C–OH (carboxyl) at 1,162 and 2,925  $\text{cm}^{-1}$ , an epoxy or alkoxy group at 1,169  $\text{cm}^{-1}$ , a broad peak due to OH groups at 3,427  $\text{cm}^{-1}$ , and C=C at 1,629.7  $\text{cm}^{-1}$  [19]. The characteristic spectra for  $\alpha\text{-Fe}_2\text{O}_3$  nanoparticles were observed at 529 and 448  $\text{cm}^{-1}$  for  $\alpha\text{-Fe}$ . The presence of glycine has characteristic peaks of C=N stretch (2,360  $\text{cm}^{-1}$ ). The FTIR spectra of FGO, characterized by the same functional groups, were observed with GO except for the characteristic peak of  $\alpha\text{-Fe}$  at 530 and 450  $\text{cm}^{-1}$ . The spectra of AFGO were characterized by increasing the number of functional groups at 2,395 and 2,919  $\text{cm}^{-1}$  that consequently helped to increase the affinity of biosorbent to adsorb large amount of dye particles.

TEM image was used to get the information about the morphology and microstructure of the GO and FGO nanocomposites. As shown in Fig. 3, the GO displays a typical flake-like and crumpled shape. The corrugation and scrolling are the intrinsic nature of GO because its ultrathin and large two-dimensional structure would become transparent and thermodynamically stable via binding Fig. 3(a). The TEM image of  $\alpha\text{-Fe}_2\text{O}_3$  nanoparticles exhibited a slender acicular shape with the major axis 39 nm (Fig. 3(b)). TEM and SEM images (Fig. 3(c)) showed the growing of  $\alpha\text{-Fe}_2\text{O}_3$  nanoparticles over the surface of GO nanosheet to form FGO nanocomposite. The SEM image of AFGO showed the presence of *A. terreus* biomass on the surface of FGO (Fig. 3(d)).

The results of BET surface area revealed that the surface area of GO nanosheet, FGO nanocomposite, and AFGO biofilm were 26.3, 148.4, and 514.3  $\text{m}^2/\text{g}$ , respectively. So, AFGO has the largest surface area due to the presence of fungus. The common analysis that is usually used for characterization of carbonaceous material is Raman spectroscopy. In the Raman spectrum of GO, the D band at 1,326  $\text{cm}^{-1}$  and the broadened G band at 1,585  $\text{cm}^{-1}$  were clearly present. On the other hand, the D band of FGO became more intense and shifted to 1,331  $\text{cm}^{-1}$  while the intensity of G band was obviously decreased and also shifted to 1,566  $\text{cm}^{-1}$  (Fig. 4). In order to estimate the degree of structural disorder, the ratio between the D and G bands (ID/IG) can be calculated. The D/G ratio of GO and FGO was 0.84 and 0.85, respectively. This meaning that they have practically identical band ration which indicate the nondestructive character during preparation method. The increasing in FGO band intensity may suggest a strong coating of hematite nanoxide on the surface of GO nanosheet.

### 3.3. Effect of pH

The biosorption process is controlled by the interaction between pH of the solution, the surface properties of the biosorbent, and the adsorbate charge. It was noted that at a low pH value (2.0), the maximum adsorption capacity of AB 25 on AFGO biofilm was  $48.5 \pm 0.5$  mg dye/g. This level dropped gradually by increasing the pH value to achieve the minimum adsorption capacity level at pH 8.

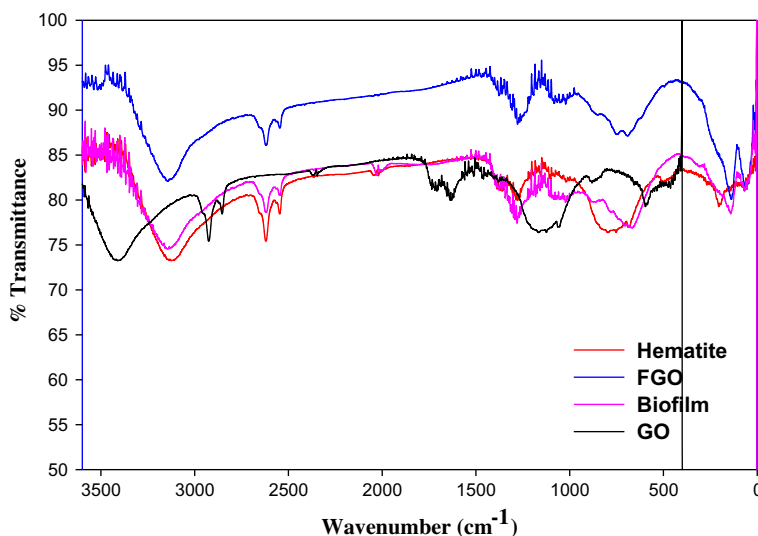


Fig. 2. FTIR spectra of prepared adsorbent at room temperature.

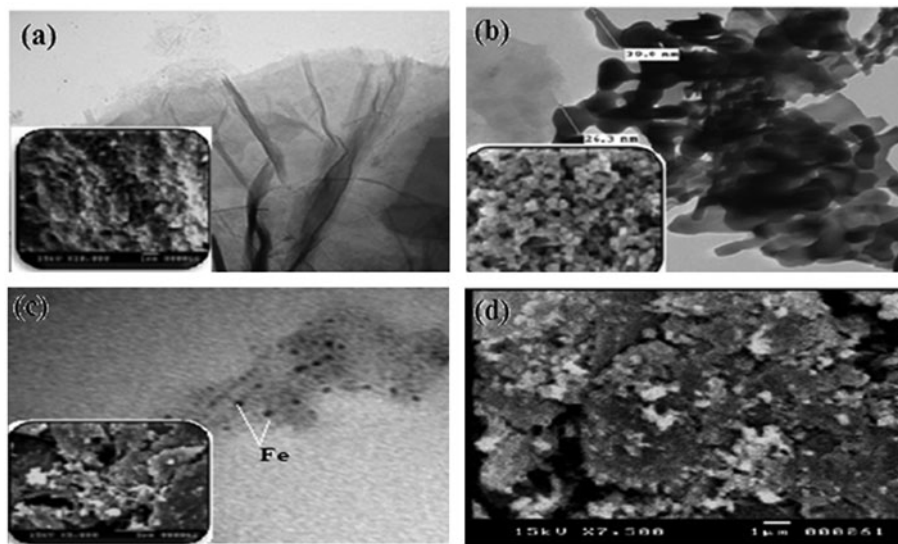


Fig. 3. SEM (interior) and TEM (exterior) images of GO (a), hematite (b), FGO (c), and AFGO (d).

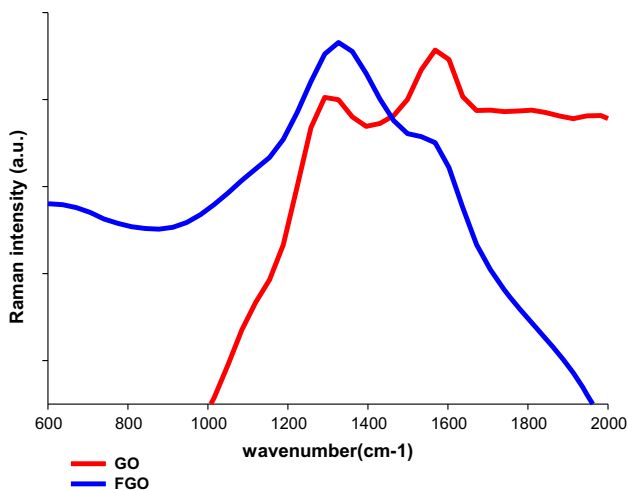


Fig. 4. Raman spectra of GO and FGO.

The cause of this observation was explained by Deller et al. [20]. The zero point of charge of GO was at pH 7.49. Below this level, it became positively charged and at the value higher than pH 7.49, it became negatively charged. The carboxylic acid and hydroxyl group are sensitive to pH alteration. The removal capability of nanocomposite slightly decreases as a function of pH due to lower dispersion of FGO nanocomposite in the aqueous solutions [21].

Moreover, at pH 2.0, the positive charges increased in the medium due to the presence of the carbonyl, carboxyl, and amine groups in the cell wall of *A. terreus*. So, the attraction mechanism between anionic

dyes and cationic surface of the biomass in acidic solutions may explain the high efficiency of dye biosorption at pH 2.0. Hydrogen ion acts as a bridging ligand between the biofilm and the dye molecule. Therefore, the interaction between anionic dyes, positive charge FGO,  $\pi$ - $\pi$  interaction, and functional group found in the fungal cell wall lead to successful adsorption of AB 25 on the biofilm.

By increasing the pH value, this mechanism became weak due to the deprotonation of the amine group which reduce the affinity of biofilm to dyes. After pH 7.0, the GO molecules and the carboxylic group became negatively charged which consequently increase the electrostatic repulsion between anionic dye and the biofilm. This result agreed with the studies of biosorption behaviors of different anionic dyes by *Aspergillus fumigatus*, *Penicillium restrictum* [22,23], GO, and FGO [24].

### 3.4. Effect of temperature

The temperature has two main effects on the adsorption processes. Increasing temperature may increase the diffusion rate of the adsorbate molecules within the pores as a result of decreasing solution viscosity and will also modify the equilibrium capacity of the adsorbent for a particular adsorbate [25]. The equilibrium biosorption capacity of AB 25 was studied at 5 constant temperatures of 5, 10, 20, 30, 40, and 50°C. At high temperature, the maximum adsorption capacity of dye was  $49.1 \pm 1.2$  mg/g. The result depicted that the adsorption capacity of AB 25

increased by increasing the temperature. The high temperature may increase the diffusion rate of the dye through the adsorbent's pore. In addition, the high temperature caused an increase in the number of energetic molecules to undergo a chemical reaction which shows chemisorption [26].

### 3.5. Adsorption studies

#### 3.5.1. Effect of contact time

The equilibrium time between the dye molecules and the adsorbent has a significant importance. The fast adsorbent is more favorable to the adsorption treatment process. Fig. 5(a) describes the effect of contact time on amount adsorption of AB 25 on AFGO. The plot in this figure could be classified into two main regions: (a) 0–50 min, which indicated the exponential dye adsorption and (b) 50–80 min, which indicate the stationary adsorption of AB 25 at equilibrium. The results showed that the time required to reach to the equilibrium was 50 min. At this time, the biofilm achieves the maximum adsorption capacity of dye (48.6 mg/g).

The dynamic changes in biosorption along the time explained that there were difference between charge density and topography and/or surface area of the used biosorbent [27,28], or by the resistance to intraparticle diffusion [29]. Increasing the adsorption capacity at the initial stage occurred due to physical adsorption, ion exchange at the cell surface or increasing the active sites on the surface of adsorbents [10,27] and the subsequent slower phase may involve other mechanisms such as complexation, micro-precipitation, or saturation of binding sites [28]. The same behavior was observed in many literatures. Gupta and Rastogi [28] reported that *Stoehospermum marginatum* could biosorb acid blue 1 within 90 min. Kyzas et al. [10] found that the GO and magnetic GO could adsorb reactive black 5 within 2 h. On the other hand, amount adsorbed of Rhodamine B on GO was 14.2 mg/g at contact time 45 min [9].

#### 3.5.2. Adsorption kinetics

It is very important to investigate the biosorption kinetics to determine which model is more suitable for

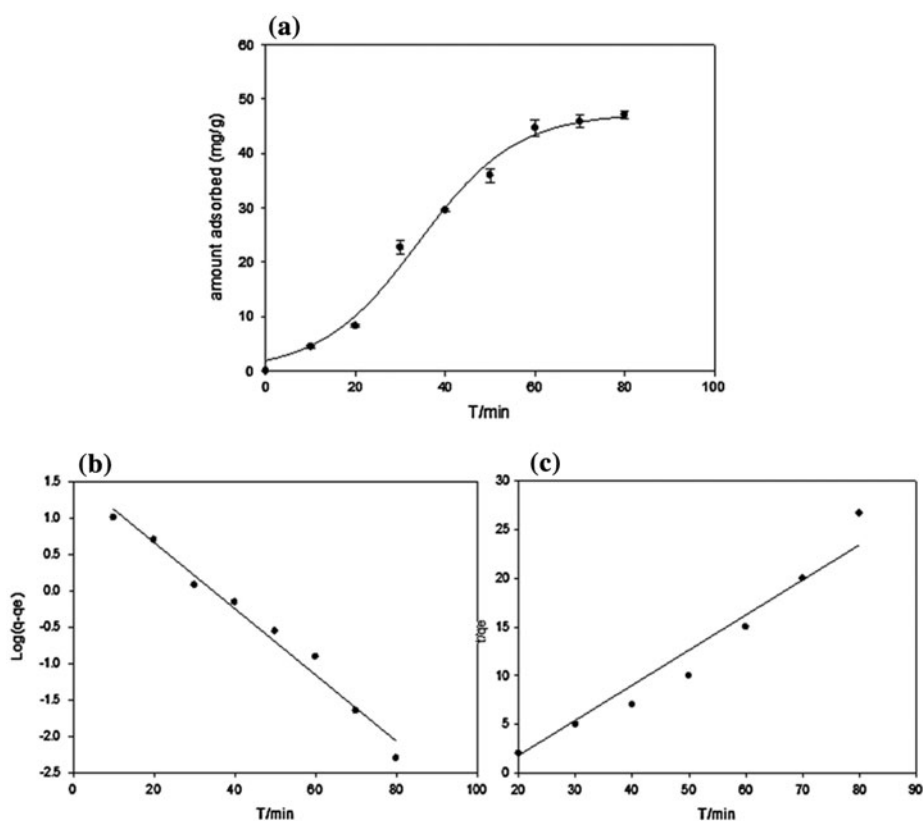


Fig. 5. Effect of contact time on adsorption of dye (a), linear form of pseudo-first-order kinetics model (b), and pseudo-second-order kinetics model (c) by AFGO at 50 mg/L AB 25, pH 2, and  $T = 30^{\circ}\text{C}$ .

description of the biosorption process. The kinetics studies were performed at the optimum pH value (2.0) and initial dye concentration 50 mg/L; the kinetics parameter of adsorption was determined by pseudo-first-order which expressed as [30]:

$$\log(q_e - q_t) = \log q_e - k_1 t/2.303 \quad (3)$$

where  $k_1$  is the pseudo-first-order rate constant and  $q_e$  and  $q_t$  are the adsorption capacity of the dye molecules on adsorbent at equilibrium and at time  $t$ , respectively. The values of  $k_1$  and  $q_e$  were evaluated by plotting  $\log(q_e - q_t)$  vs. the time and the calculated  $q_e$  are demonstrated in Fig. 5(b). The amount adsorbed of AB 25 on the biofilm was  $48.6 \pm 1.8$  (mg/g) when the  $R^2$  value of the plot was 0.98 and  $k_1$  was  $0.017 \pm 0.014$ . The calculated  $q_e$  value seemed to be much closed to the experimental one ( $46.62 \pm 0.9$ ) (Fig. 5(a)).

The linear form of pseudo-second-order kinetics model was presented by the equation [31]:

$$t/q = 1/k_2 q_e^2 + t/q_e \quad (4)$$

where  $k_2$  was the pseudo-second-order adsorption rate constant. The values of  $k_2$  and  $q_e$  were estimated from the slope and intercept of plots of  $t/q_e$  vs.  $t$  (Fig. 5(c)). It is observed that the range  $R^2$  value was 0.95 and the calculated  $q_e$  and  $k_2$  were  $2.8 \pm 0.2$  mg/g and  $0.002 \pm 0.001$ . The value of calculated  $q_e$  was lower than the experimental value.

So, the pseudo-first-order model was more fitted to the adsorption of AB 25 on AFGO. Adsorption kinetics explains how fast the sorption process occurs and also the factors affecting the reaction rate. The nature of sorption will depend on the physical or chemical characteristics of the adsorbent system and also on the system conditions [32]. So, the given data suggesting the chemisorption behavior of AB 25 on the surface AFGO because it followed pseudo-second-order model. These results came in the context with many literatures which discussed the absorption kinetics of different textile dyes by GO and  $\text{Fe}_3\text{O}_4/\text{GO}$  [8,10]. Other literature discussed the kinetics models varied according to the type of dye and the type of carbonaceous adsorbent such as removal of Novacron orange P-2R by sugarcane bagasse [33].

### 3.5.3. Adsorption isotherm

The batch adsorption isotherm experiments were carried out at the different AB 25 concentration range from 20 to 300 mg/L to investigate the electrostatic nature of the adsorbate-biosorbent interaction

Fig. 6(a). Langmuir model assumed that one adsorbate molecule interacts with only one binding site of the adsorbent to form monolayer adsorption. The data were analyzed using the linear form of Langmuir isotherm model (Fig. 6(b)) which is expressed as the following equation [9]:

$$C_e/q_e = 1/q_{\max} b + C_{eq}/q_{\max} C_e \quad (6)$$

where  $b$  is the Langmuir constant related to the affinity between an adsorbate and biosorbent and  $q_{\max}$  is the maximum monolayer adsorption capacity. These values were calculated from the slope and intercept of the linear plot of  $C_e/q_e$  against  $C_e$ . The calculated  $q_{\max}$  and  $b$  values were 168.3 mg/g and 0.05, respectively.

Freundlich is more complicated adsorption model which deals with adsorption of dye on the heterogeneous surface. The linear form of this model is expressed by the following equation [34]:

$$\ln q_e = (1/n) \ln C_e + \ln K_f \quad (7)$$

where  $K_f$  and  $n$  are the adsorption capacity and the intensity of adsorption, respectively. By plotting the  $\ln q_e$  vs.  $\ln C_e$  (Fig. 6(c)). The estimated value of  $n$  was 1.93 and  $K_f$  was 4,142.6. The previous results showed that the Langmuir adsorption isotherm ( $R^2 = 0.99$ ) was the most favorable model for biosorption of AB 25 on the biofilm rather than Freundlich ( $R^2 = 0.96$ ). By increasing the concentration of AB 25, the adsorption capacity increased. This meaning that the biosorption process takes place through formation of monolayer on the surface of AFGO biofilm. Because at low concentration of dye, the fast saturation of the surface due to fast uptake of dye while at high concentration dyes, molecules need to diffuse on the surface of biosorbent and highly hydrolyzed molecules will be diffused with slow rate [35]. The value of maximum adsorption capacity for adsorption of AB 25 on AFGO was higher than the value for adsorption of direct violet 51 (39.6 mg/g) on sugarcane bagasse treated with HCl [36]. In addition, when comparing the  $q_{\max}$  for adsorption of AB 25 in this study by other studies investigated by Zaheer et al. [37] for biosorption of Foron Blue E-BL on the surface of native, immobilized, and pretreated sugarcane bagasse, the adsorbent in the present study is more favorable for adsorption.

### 3.6. Thermodynamics

The adsorption thermodynamics were analyzed based on the adsorption isotherm of AB 25, thermodynamic parameters give the detailed information about

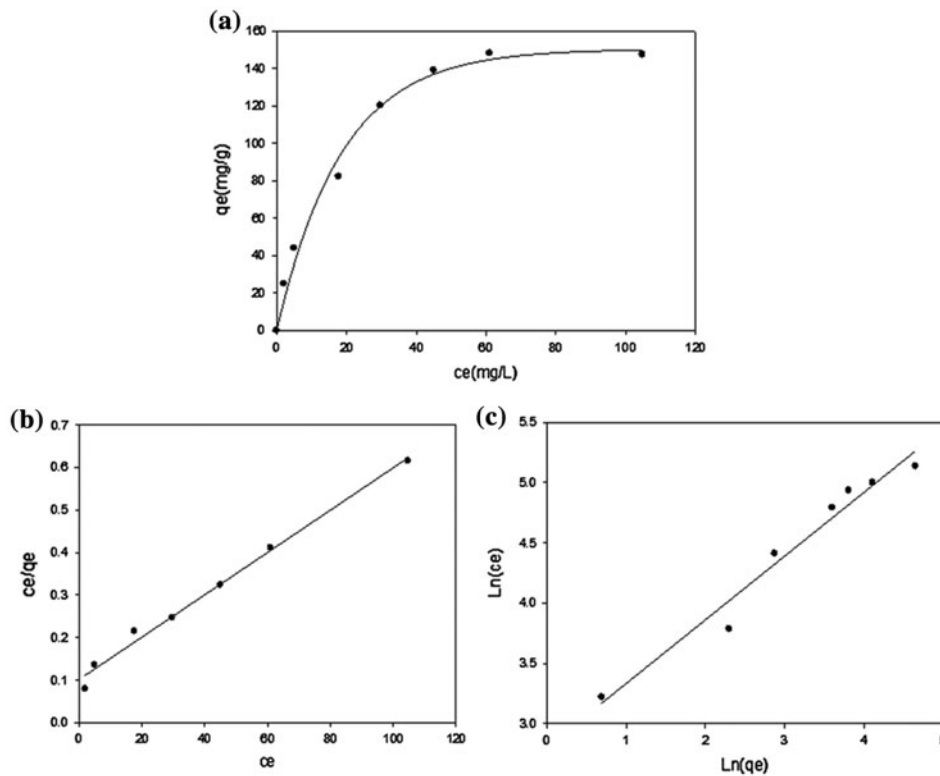


Fig. 6. Experimental data of adsorption isotherm (a), linear form of Langmuir (b), and Freundlich (c) adsorption isotherm models at 50 mg/L AB 25, pH 2, and  $T = 30^\circ\text{C}$ .

the change of energy during the adsorption process. The Gibbs free energy change,  $\Delta G^\circ$  (kJ/mol), of the adsorption process is related to the distribution coefficient ( $K$ ) by the Van't Hoff equation (where  $R$  is the universal gas constant and is equal to 8.314 J/mol K) [38], enthalpy change ( $\Delta H^\circ$ ), and entropy change ( $\Delta S^\circ$ ) of biosorption of AB 25 on AFGO. These parameters were calculated according the following equation:

$$\Delta G^\circ = -RT \ln(k_c) \quad (8)$$

$$k_c = q_e/C_e \quad (9)$$

$$\Delta G^\circ = \Delta H^\circ - T\Delta S^\circ \quad (10)$$

$$\ln k_c = \Delta S^\circ/R - \Delta H^\circ/RT \quad (11)$$

The thermodynamics parameters were performed at 50 mg/L of AB 25 and pH 2.0. Van't Hoff plot was performed by plotting  $\ln k_c$  vs.  $1/T$ .  $\Delta H^\circ$  and  $\Delta S^\circ$  were estimated from the slope and intercept of this plot.  $\Delta H$ ,  $\Delta S^\circ$ , and  $R^2$  values were 9.37, -226.6, and 0.97 as listed in Table 1. It was observed that the positive values of  $\Delta G^\circ$  appeared at the temperature below  $20^\circ\text{C}$

indicated that at low temperature, the adsorption process may be non-spontaneous. By increasing the temperature from 5 to  $20^\circ\text{C}$ , the  $\Delta G^\circ$  value decreased.

After  $20^\circ\text{C}$ ,  $\Delta G^\circ$  was negative, and values indicated the adsorption process carried out spontaneously on the surface of the biofilm. It was also observed that by increasing the temperature, the negative value of  $\Delta G^\circ$  increased and implied that lower temperature may ease the biosorption process. The negative value of  $\Delta H^\circ$  indicated the process was exothermic, thereby illustrating that the process was energetically stable. The exothermic process implied that total energy

Table 1

The thermodynamic parameters of AB 25 biosorption on AFGO biofilm

$T$ ( $^\circ\text{C}$ )	$\Delta G$ (kJ/mol)	$\Delta S^\circ$	$\Delta H^\circ$
5	180.5984	$9.37 \pm 0.85$	-226.6
10	134.5446		
20	42.43701		
30	-49.6706		
40	-141.778		
50	-325.993		

released in bond making between AB 25 and AFGO is more than the total energy absorbed in bond breaking. This process has enabled releasing of extra energy in the form of heat, and then  $\Delta H^\circ$  became negative.

Moreover, the positive value of  $\Delta S^\circ$  suggested the biosorption process was entropy driven. Generally, the positive value of  $\Delta S^\circ$  indicated the increase in the disorder at solid/liquid interface making the adsorbate (AB 25) ions or molecules to move quickly from the liquid phase to the solid one. Therefore, the amount adsorbed enhanced and increased.

Many literature proved that the biosorption of different dyes on different biosorbents was exothermic and spontaneous as adsorption of Drimarene Blue HF-RL on the surface of immobilized peanut hulls [39] and Foron Blue E-BL on sugarcane bagasse [37].

During the adsorption, the coordinated water molecules (which are displaced by the dye molecules) gain more translational entropy than is lost by the dye molecules, resulting in increased randomness in the dye-adsorbent interaction [40]. It is well known that ionic dyes tend to aggregate in dilute solutions, leading to the dimer formation [41]. It is supposed that the dimer formation in solution is mainly due to hydrophobic interactions or permanent and transition dipole moments [41]. Although dyes are very individualistic in structure, certain broad rules are well established regarding their dimerization. The probability increases with an increase in dye concentration or ionic strength; it will decrease with the rise of temperature or the addition of organic solvents [42].

#### 4. Conclusion

*A. terreus* was isolated from the industrial effluent sample.  $\alpha$ -Fe<sub>2</sub>O<sub>3</sub>/GO nanocomposite (FGO) was synthesized by the impregnation method. The usage of FGO nanocomposite as a supporting material for *A. terreus* AUMC-10516 (in a form of biofilm (AFGO)) is a new approach. This biofilm showed high performance in the adsorption of anthraquinone dye (AB 25) from aqueous solution. Because of increasing the active functional groups on the surface of AFGO biofilm as well as increasing its surface area which make it more susceptible for adsorb a large amount of dye molecules. The low pH value at 2.0 was the best medium for adsorption of AB 25. The time required to achieve the maximum adsorption capacity (48.6 mg/g) to reach the equilibrium was at 50 min. The adsorption kinetics analysis revealed that the adsorption of AB 25 was controlled by pseudo-second-order model. The adsorption isotherm of AB 25 on AFGO was monolayer and followed the Langmuir model which

indicates the reaction was fast biosorption rate. The biosorption process carried out spontaneously with exothermic attitude.

#### Acknowledgment

This work is financially supported by Botany and Microbiology Department, Faculty of Science, Assiut University. The authors also gratefully acknowledge the supports in EM, XRD, and FTIR measurements and valuable suggestions by Dr Sedky Hassan.

#### References

- [1] I.A. Aguayo-Villarreal, V. Hernández-Montoya, A. Bonilla-Petriciolet, R. Tovar-Gómez, E.M. Ramírez-López, M.A. Montes-Morán, Role of acid blue 25 dye as active site for the adsorption of Cd<sup>2+</sup> and Zn<sup>2+</sup> using activated carbons, *Dyes Pigment.* 96 (2013) 459–466.
- [2] L. Sendelbach, A review of the toxicity and carcinogenicity of anthraquinone derivatives, *Toxicology* 57 (1989) 227–240.
- [3] R. Schneider, Effects of nonpathogenic strains of *Fusarium oxysporum* on celery root infection by *F. oxysporum* f. sp. *apii* and a novel use of the Lineweaver-Burk double reciprocal plot technique, *Phytopathology* 74 (1984) 646–653.
- [4] G. Wilkinson, Statistical estimations in enzyme kinetics, *Biochem J.* 80 (1961) 315–324.
- [5] Y. Suzuki, T. Yoda, A. Ruhul, W. Sugiura, Molecular cloning and characterization of the gene coding for azoreductase from *Bacillus* sp. OY1-2 isolated from soil, *J. Biol. Chem.* 276 (2001) 9059–9065.
- [6] A. Stolz, Basic and applied aspects in the microbial degradation of azo dyes, *Appl. Microbiol. Biotechnol.* 56 (2001) 69–80.
- [7] H. Chen, S.L. Hopper, C.E. Cerniglia, Biochemical and molecular characterization of an azoreductase from *Staphylococcus aureus*, a tetrameric NADPH-dependent flavoprotein, *Microbiology* 151 (2005) 1433–1441.
- [8] P. Sharma, M.R. Das, Removal of a cationic dye from aqueous solution using graphene oxide nanosheets: Investigation of adsorption parameters, *J. Chem. Eng. Data* 58 (2012) 151–158.
- [9] I. Langmuir, The adsorption of gases on plane surfaces of glass, mica and platinum, *J. Am. Chem. Soc.* 40 (1918) 1361–1403.
- [10] G.Z. Kyzas, N.A. Travlou, O. Kalogirou, E.A. Deliyanni, Magnetic graphene oxide: Effect of preparation route on reactive black 5 adsorption, *Materials* 6 (2013) 1360–1376.
- [11] Y. Zhu, S. Murali, W. Cai, X. Li, J.W. Suk, J.R. Potts, R.S. Ruoff, Graphene and graphene oxide: Synthesis, properties, and applications, *Adv. Mater.* 22 (2010) 3906–3924.
- [12] R. Saratale, G. Saratale, D. Kalyani, J.-S. Chang, S. Govindwar, Enhanced decolorization and biodegradation of textile azo dye Scarlet R by using developed microbial consortium-GR, *Bioresour. Technol.* 100 (2009) 2493–2500.

- [13] Z. Aksu, Ş.Ş. Çağatay, Investigation of biosorption of Gemazol Turquoise Blue-G reactive dye by dried *Rhizopus arrhizus* in batch and continuous systems, *Sep. Purif. Technol.* 48 (2006) 24–35.
- [14] S. Ong, E. Toorisaka, M. Hirata, T. Hano, Combination of adsorption and biodegradation processes for textile effluent treatment using a granular activated carbon-biofilm configured packed column system, *J. Environ. Sci.* 20 (2008) 952–956.
- [15] K. Kloos, J.C. Munch, M. Schloter, A new method for the detection of alkane-monooxygenase homologous genes (alkB) in soils based on PCR-hybridization, *J. Microbiol. Methods* 66 (2006) 486–496.
- [16] S. Dağdelen, B. Acemioğlu, E. Baran, O. Koçer, Removal of remazol brilliant blue R from aqueous solution by pirina pretreated with nitric acid and commercial activated carbon, *Water Air Soil Pollut.* 225 (2014) 1–15.
- [17] R.M. Gabr, S.M. Gad-Elrab, R.N. Abskharon, S.H. Hassan, A.A. Shoreit, Biosorption of hexavalent chromium using biofilm of *E. coli* supported on granulated activated carbon, *World J. Microbiol. Biotechnol.* 25 (2009) 1695–1703.
- [18] A.M.M. Mawad, N.M.H. Yousef, A.A.M. Shoreit, Bioremediation of acid blue 25 dye by anthracene degrading *Pseudomonas pseudoalcaligenes* ASU-016, *Catrina: Int. J. Environ. Sci.* 10 (2015) 53–60.
- [19] J.-S. Chang, C. Chou, S.-Y. Chen, Decolorization of azo dyes with immobilized *Pseudomonas luteola*, *Process Biochem.* 36 (2001) 757–763.
- [20] S. Deller, S. Sollner, R. Trenker-El-Toukhy, I. Jelesarov, G.M. Gübitz, P. Macheroux, Characterization of a thermostable NADPH: FMN oxidoreductase from the mesophilic bacterium *Bacillus subtilis*, *Biochemistry* 45 (2006) 7083–7091.
- [21] K. Meral, Ö. Metin, Graphene oxide–magnetite nanocomposite as an efficient and magnetically separable adsorbent for methylene blue removal from aqueous solution, *Turk. J. Chem.* 38 (2014) 775–782.
- [22] M. Nakanishi, C. Yatome, N. Ishida, Y. Kitade, Putative ACP phosphodiesterase gene (acpD) encodes an azoreductase, *J. Biol. Chem.* 276 (2001) 46394–46399.
- [23] N. Supaka, K. Juntongjin, S. Damronglerd, M.-L. Delia, P. Strehaiano, Microbial decolorization of reactive azo dyes in a sequential anaerobic–aerobic system, *Chem. Eng. J.* 99 (2004) 169–176.
- [24] N.A. Travlou, G.Z. Kyzas, N.K. Lazaridis, E.A. Deliyanni, Graphite oxide/chitosan composite for reactive dye removal, *Chem. Eng. J.* 217 (2013) 256–265.
- [25] G. Cengiz, P. Aytar, M. Şam, A. Çabuk, Removal of reactive dyes using magnetically separable trames versicolor cells as a new composite biosorbent, *Sep. Sci. Technol.* 49 (2014) 1860–1871.
- [26] J.Y. Farah, N.S. El-Gendy, L.A. Farahat, Biosorption of Astrazone Blue basic dye from an aqueous solution using dried biomass of Baker’s yeast, *J. Hazard. Mater.* 148 (2007) 402–408.
- [27] E. Daneshvar, M. Kousha, M.S. Sohrabi, A. Khataee, A. Converti, Biosorption of three acid dyes by the brown macroalga *Stoehospermum marginatum*: Isotherm, kinetic and thermodynamic studies, *Chem. Eng. J.* 195–196 (2012) 297–306.
- [28] V. Gupta, A. Rastogi, Biosorption of hexavalent chromium by raw and acid-treated green alga *Oedogonium hatei* from aqueous solutions, *J. Hazard. Mater.* 163 (2009) 396–402.
- [29] Z. Aksu, S. Tezer, Biosorption of reactive dyes on the green alga *Chlorella vulgaris*, *Process Biochem.* 40 (2005) 1347–1361.
- [30] S. Largergren, Zur theorie der sogenannten adsorption gelöster stoffe (On the theory of so-called Adsorption of dissolved substances), *Kungliga Svenska Vetenskapsakademiens. Handlingar*, 24 (1898) 1–39.
- [31] Y.-S. Ho, G. McKay, Pseudo-second order model for sorption processes, *Process Biochem.* 34 (1999) 451–465.
- [32] O. Anjaneya, M. Santoshkumar, S.N. Anand, T. Karegoudar, Biosorption of acid violet dye from aqueous solutions using native biomass of a new isolate of *Penicillium* sp, *Int. Biodeterior. Biodegrad.* 63 (2009) 782–787.
- [33] S. Noreen, H.N. Bhatti, Fitting of equilibrium and kinetic data for the removal of Novacron Orange P-2R by sugarcane bagasse, *J. Ind. Eng. Chem.* 20 (2014) 1684–1692.
- [34] U. Freundlich, Die adsorption in lösungen (The adsorption in solutions), *J. Phys. Chem. (Leipzig)*, 57 (1906) 385–470.
- [35] J.-H. Joo, S.H. Hassan, S.-E. Oh, Comparative study of biosorption of  $Zn^{2+}$  by *Pseudomonas aeruginosa* and *Bacillus cereus*, *Int. Biodeterior. Biodegrad.* 64 (2010) 734–741.
- [36] S. Sadaf, H.N. Bhatti, S. Nausheen, S. Noreen, Potential use of low-cost lignocellulosic waste for the removal of direct violet 51 from aqueous solution: Equilibrium and breakthrough studies, *Arch. Environ. Contam. Toxicol.* 66 (2014) 557–571.
- [37] S. Zaheer, H. Bhatti, S. Sadaf, Y. Safa, M. Zia-ur-Ruhman, Biosorption characteristics of sugarcane bagasse for the removal of foron blue E-BL dye from aqueous solutions, *J. Animal Plants Sci.* 24 (2014) 272–279.
- [38] T. Robinson, G. McMullan, R. Marchant, P. Nigam, Remediation of dyes in textile effluent: A critical review on current treatment technologies with a proposed alternative, *Bioresour. Technol.* 77 (2001) 247–255.
- [39] S. Noreen, H.N. Bhatti, S. Nausheen, M. Zahid, S. Asim, Biosorption of Drimarine Blue HF-RL using raw, pretreated, and immobilized peanut hulls, *Desalin. Water Treat.* 52 (2014) 7339–7353.
- [40] Y. Miao, Biological remediation of dyes in textile effluent: A review on current treatment technologies, 2005. Retrieved 28 July, 2011, from: <<http://home.eng.ias.tate.edu/~tge/ce421-521/yongjie.pdf>>.
- [41] L. Morais, O. Freitas, E. Gonçalves, L. Vasconcelos, C.G. Beca, Reactive dyes removal from wastewaters by adsorption on eucalyptus bark: Variables that define the process, *Water Res.* 33 (1999) 979–988.
- [42] K.R. Ramakrishna, T. Viraraghavan, Dye removal using low cost adsorbents, *Water Sci. Technol.* 36 (1997) 189–196.